



**Tailoring Mechanical Response through Coronal Layer
Overlap in Tethered Micelle Hydrogel Networks**

Journal:	<i>Soft Matter</i>
Manuscript ID:	SM-ART-01-2015-000122.R1
Article Type:	Paper
Date Submitted by the Author:	23-Mar-2015
Complete List of Authors:	Guo, Chen; Colorado State University, Chemical and Biological Engineering Bailey, Travis; Colorado State University, Chemical and Biological Engineering

Cite this: DOI: 10.1039/c0xx00000x

www.rsc.org/xxxxxx

ARTICLE

Tailoring Mechanical Response through Coronal Layer Overlap in Tethered Micelle Hydrogel Networks

Chen Guo^a and Travis S. Bailey^{a,b}*Received (in XXX, XXX) Xth XXXXXXXXX 20XX, Accepted Xth XXXXXXXXX 20XX*

DOI: 10.1039/b000000x

Tethered micelle hydrogel networks based on the solution assembly of amphiphilic ABA-type block copolymers are prevalent throughout the hydrogel literature. However, the mechanical response of such systems is often determined largely by the integrity of the micellar core produced during solution assembly, not by the elements of the network structure upon which it is based. Using a solvent-free fabrication method based on the melt-state self-assembly of sphere-forming polystyrene-*b*-poly(ethylene oxide) (SO) diblock and SOS triblock copolymers blends, we have been able to produce tethered micelle hydrogel networks with fully vitrified cores that enable the elements of the network structure to determine the mechanical response. Here, we explore the impact of using PEO midblocks of different lengths within the SOS tethers, in an effort to elucidate the role played by water content, tether concentration, and tether length in mechanical property determination. In doing so, we were able to establish coronal layer overlap as the primary contributing factor in regulating the dynamic elastic moduli exhibited by tethered micelle systems. Variation of either tether concentration or tether length could be used to tune the degree of coronal layer overlap, enabling direct and accurate control over hydrogel mechanical response. While such control is likely a unique feature of the melt-state fabrication approach applied here, the conclusions with respect to the role of coronal layer overlap and tether (bridging) concentration in determining the mechanical potential of the network should be applicable to all ABA-type tethered micelle systems, regardless of fabrication methodology.

Introduction

Polymer-based hydrogel networks have become increasingly important targets for a range of applications beyond simple commodity based absorbents, such as wound dressings, chemical and drug delivery agents, tissue growth scaffolds, ocular lenses, and biomedical-related implant technologies. However, extension to these types of applications requires hydrogel designs through which functionality, biocompatibility, mass transport and mechanical response can be carefully tailored to meet highly specific performance criteria.¹⁰ At the center of this development challenge lays the need for synthetic protocols capable of producing basic hydrophilic polymer networks with spatial homogeneity at length scales in the nanoscale range, where precision, accuracy, and reproducibility of performance are ultimately determined.

Producing networks with submicron homogeneity in mesh size can be challenging using traditional crosslinking of multifunctional monomer, oligomer, or polymer chains. The use of tethered micelle networks formed from solution-based self-assembly of amphiphilic ABA triblock copolymers has been one of the most prevalent alternate strategies explored over the last decade, particularly as injectable media for local delivery of

therapeutics. Using the micelle morphology as a fundamental structural unit provides a number of unique opportunities not available in traditional systems fabricated from simple crosslinking of hydrophilic polymers. Notably, each micelle becomes a multifunctional junction point within the network, comprised of hundreds of chains, many of which form bridges or tethers to adjacent micelle junction points. Thus, the number of effective network strands between junction points can be quite large, providing a potential to produce very mechanically robust materials. Unfortunately, the mechanical properties of tethered micelle networks formed are often limited in practice, a consequence of the limited micelle core integrity achievable during the solution-based fabrication methods used to produce them. For applications such as controlled or targeted delivery through an injectable medium, the ability to plastically deform such materials can provide a distinct advantage for post injection molding, for example. However, our group has been focused on ways to tap the intrinsic potential of the tethered micelle framework to produce more mechanically robust hydrogel constructs, ones capable of reproducing, for example, the mechanical function exhibited by biologically derived hydrated soft tissues.

Tethered micelle network formation is typically accomplished

through the use of solvated ABA systems in which the A blocks can be thermodynamically triggered to phase separate (precipitate) out of solution, producing spherical micelle aggregates containing (hydrophobic) collapsed cores of polymer A and (hydrophilic) coronal layers of solvated polymer B. If the concentration of the polymer in solution is low, precipitating block copolymers form flower-like micelles characterized by looping chains, in which opposite ends of a chain predominantly occupy the same micelle core. When the concentration of ABA triblock exceeds a critical value, a sufficient fraction of opposing chains ends form bridges between adjacent micelle cores, and an infinite network of tethered micelles is formed. Not surprisingly, bridging fractions, micelle size distribution, aggregation number, and network uniformity can all be quite sensitive to changes in concentration, precipitation kinetics, differences in solvent selectivity between blocks, and the rate at which the conditions for precipitation are invoked. An inability to control such factors is one facet of tethered micelle network synthesis that makes optimizing mechanical properties in these systems difficult. However, in most cases, the mechanical deficiency of these network materials can almost always be traced to the limited mechanical integrity of the micelle cores formed during the precipitation step.^{5, 11, 12, 13} As the formal junction points through which stress is distributed across the hydrogel, the physical state of the micelle core is central to the mechanical potential of the network. In some cases, small aggregation numbers in the tens of chains are not of sufficient size to produce bulk-like mechanical properties. In other cases, residual solvent trapped during chain aggregation effectively plasticizes the micelle core, a kinetic problem faced even in systems for which very sharp thermodynamic transitions in chain end solubility have been achieved. Successful attempts to improve the mechanical stability have involved integration of chain end blocks for which post-precipitation crystallization or cross-linking is possible. For example, dramatic improvements in mechanical response have been achieved through in situ cross-linking of micelle cores composed of functionalized polylactides.¹⁴ However, these examples are few, and the promise of solution assembly as a generalized means to tethered micelle networks of extensive mechanical elasticity, strength, and toughness appears limited.

Our group has been exploring the use of solvent free assembly of tethered micelle networks as a route to hydrogel materials of improved mechanical (and chemical) function. Recently,¹⁵ we introduced a novel approach exploiting the self-assembly of sphere-forming block copolymers, allowing us to establish the tethered micelle network in the melt-state, sans solvent. Self-assembly in the melt state permits pre-structuring of the network prior to swelling, in direct contrast with the majority of hydrogel preparations.^{1, 7, 9, 11, 14, 16} Either vitrification¹⁵ or chemical crosslinking¹⁷ of the spherical domains following self-assembly can be used to fix the network structure, prior to the introduction of a matrix selective solvent. Because of the very high bridging fractions found in sphere-based ABA block copolymer morphologies (approaching 80%)¹⁸, we found we could introduce considerable amounts of non-tethering AB diblock copolymer (up to 96.7 mol%) to the standard ABA triblock copolymer systems and still achieve infinitely tethered networks. This is a direct consequence of the very high aggregation numbers found in

sphere based block copolymer morphologies. For example, in polystyrene-poly(ethylene oxide) (PS-PEO, SO) diblock and PS-PEO-PS (SOS) triblock copolymer blends used as a model system in our previous work, each spherical domain was found to have a mean aggregation number of over 200 PS chains. With high bridging fractions, and only several bridging chains per sphere necessary to reach the infinite network gel point¹⁹, very little SOS triblock copolymer was actually required to form infinitely connected systems.

We found that this fabrication strategy could produce hydrogels with dynamic elastic moduli tunable from 100 Pa to 100 kPa simply through adjustment of SOS triblock copolymer content. Compressive moduli could similarly be tuned from 7.5 kPa to over a 1000 kPa, and swelling ratios (Q), from 35.5 g water/g polymer (at 20 °C) down to 5.0 g water/g polymer. This dramatic tunability was all possible by simply changing the amount of SOS triblock copolymer in the system. And while the improvements gained relative to solution assembled systems were impressive, how these properties correlated to changes in network structure was not particularly obvious. For example, at a fixed temperature, there did appear to be a clear (and not particularly interesting) relationship: more tethers, less solvent, higher modulus. This seemed to be in general agreement with what would be expected for an ideal swollen elastomer, in which

$$\text{Modulus} \propto T \cdot \phi_2^{1/3} \cdot (v_e/V_0)$$

where T is absolute temperature, ϕ_2 is the volume fraction of polymer in the swollen state, and (v_e/V_0) is the effective number of cross-linking strands (polymer chains spanning two junction points) per unit volume of the unswollen dry polymer. However, in taking advantage of the decreasing solubility of PEO in water with increasing temperature, we found we could decrease the swelling ratio by as much as 33% simply by heating the hydrogels from 10°C to 50°C. In doing so, however, we found that the mechanical properties of the system remained essentially unchanged, despite the increases in both T and ϕ_2 . Furthermore, we found that the addition of SOS triblock copolymer tethers appeared to increase modulus at a much faster rate than expected, such that each additional SOS triblock copolymer molecule added was acting to create more than one additional effective strand. So although we could see there were evident correlations between SOS triblock copolymer concentration, equilibrium swelling ratio, and mechanical performance, our understanding of the origin of the mechanical properties in these tethered micelle networks remained quite limited.

In this report, we have expanded our investigation of the model SO/SOS systems in an attempt to resolve the degree to which the various structural elements are contributing to the mechanics of these melt-prestructured tethered micelle networks. In the previously described model SO/SOS system, the SOS triblock copolymer used was always twice the molecular weight of the SO diblock copolymer, such that their preferred lattice dimensions during self-assembly were "matched". Here, we introduce SOS triblock copolymer for which the PEO midblock has been extended in molecular weight relative to the length generated by simply coupling SO diblock copolymer. As shown in Figure 1, the study revolves around hydrogels produced from three blends

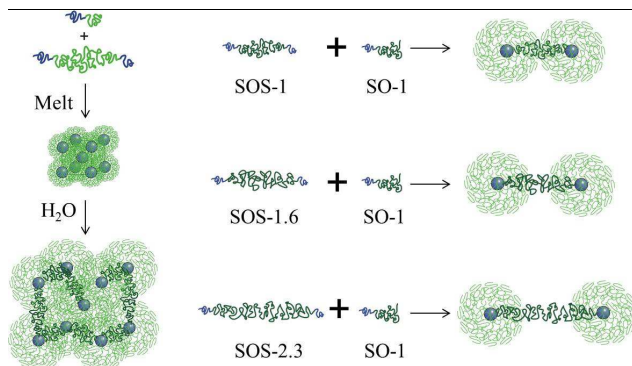


Figure 1. Illustration showing the use of sphere-forming AB diblock and ABA triblock copolymer blends to prestructure tethered micelle networks in the absence of solvent (left). In this study, the molecular weight of the bridging tethers is varied help expose the contribution of various structural elements towards the resultant hydrogel mechanics.

involving distinct pairings of a single SO diblock copolymer and three different SOS triblock copolymer molecules. Importantly, the SO diblock copolymer was kept identical throughout the series, and the PS chain ends for all molecules originate from the same PS-OH parent block. Thus, the PEO midblock molecular weight is designed as the only variable among blends of similar SO:SOS molar ratios. Each SOS triblock copolymer is designated as SOS-Y, where Y is the ratio of the PEO midblock molecular weight present in the SOS-Y triblock copolymer relative to midblock molecular weight if the SOS triblock copolymer were "matched".

The premise behind studying these three sets of blends is tied to the tether's critical role in determining the equilibrium swelling dimensions of the hydrogel. At low SOS concentrations, the equilibrium swelling dimensions are determined by the balance of solvent-induced osmotic swelling force trying to disperse the micelles, and the entropic restoring force of the tethering midblocks which resist chain stretching associated with the swelling process. As concentrations of tethering midblocks increase, topologically constrained entanglements among the tethers restrict swelling even further. The increasing number of entanglements is responsible for the decreased swelling ratios produced at higher SOS concentrations. By increasing the tether lengths exclusively, we hypothesized we could increase the swelling ratio independently from SOS triblock copolymer concentration, providing a means of decoupling the mechanical contributions of those two quantities. As we show within, it is actually the degree of coronal overlap dictated by the length and quantity of tethers that is the major contributor to the mechanics of the hydrogel network. Notably, the use of melt-state prestructuring (in contrast to solution assembly) provides the means to accurately control both.

Experimental

Materials. Styrene (99%, 4-tert-butylcatechol inhibitor, Aldrich) and ethylene oxide (99.5+%, compressed gas, Aldrich) monomer were each purified by successive vacuum distillations (10–20 mTorr) from dried dibutylmagnesium (0.1 mmol g⁻¹ monomer, 1.0M solution in heptane, Aldrich) before use. Both purified styrene and ethylene oxide monomer were stored in glass

burettes in the dark, at room temperature (styrene) and 0 °C (ethylene oxide), respectively, until use (typically less than 24 h). Argon degassed cyclohexane (CHX) was purified by passing the solvent over activated alumina followed by Q-5-like supported copper catalyst (Glass Contour, proprietary). Argon degassed tetrahydrofuran (THF) was purified by passing the solvent over activated alumina. High-purity argon (99.998%, Airgas) was passed through additional oxygen and moisture traps prior to use. Glassware and polymerization reactors were flamed under vacuum and backfilled with argon (3x). Materials added to the reactors were added while Ar was blowing for all air-free chemical reactions. All other materials were used as received.

ω-Hydroxyl-polystyrene (S-OH) S-OH was prepared as described previously^{15, 20} using anionic polymerization of polystyrene followed by quantitative hydroxyl functionalization using ethylene oxide. SEC (THF, PS std): $M_n=8390$ g mol⁻¹, $M_w=8660$ g mol⁻¹, $M_w/M_n=1.03$. δH (300MHz, CDCl₃): 6.20–7.26 (br, $-C_6H_5$), 3.2–3.5 (m, $-CH_2OH$), 0.84–2.60 (br, $-CH(C_6H_5)CH_2-$, $CH_3CH(CH_2CH_3)-$, $-CH_2CH_2OH$), 0.5–0.78 (m, $CH_3CH(CH_2CH_3)-$).

ω-Hydroxyl-polystyrene-b-poly(ethylene oxide) (SO-1, SO-1.6, SO-2.3). SO-1, SO-1.6 and SO-2.3 were prepared as described previously¹⁵ by treating different amounts of S-OH (SO-1: 3.71 g, 0.442 mmol; SO-1.6: 0.6 g, 0.072 mmol; SO-2.3: 1.128 g, 0.134 mmol) with potassium naphthalenide to generate the alkoxide macroinitiator and adding ethylene oxide (SO-1: 29.9 g, 0.679 mol; SO-1.6: 11.1 g, 0.252 mol; SO-2.3: 21.6 g, 0.488 mol, 0 °C) accordingly. For SO-1, Yield 32.4 g, 96.4%. SEC (THF, PS std.): $M_w/M_n=1.026$, $M_n=84380$ g mol⁻¹ (calculated using ¹H-NMR and SEC measured S-OH M_n). For SO-1.6, Yield 7.27 g, 63.0%. SEC (THF, PS std.): $M_w/M_n=1.040$, $M_n=129658$ g mol⁻¹ (calculated using ¹H-NMR and SEC measured S-OH M_n). For SO-2.3, Yield 20.16 g, 89.1%. SEC (THF, PS std.): $M_w/M_n=1.148$, $M_n=183201$ g mol⁻¹ (calculated using ¹H-NMR and SEC measured S-OH M_n). δH (400MHz, CDCl₃): 6.20–7.26 (br, $-C_6H_5$), 4.55 (s, $-OCH_2(C_6H_4)CH_2O-$), 3.1–4.0 (br, $-CH_2CH_2O-$, $-CH(C_6H_5)CH_2CH_2O-$), 1.0–2.30 (br, $-CH_2CH(C_6H_5)-$, $CH_3CH(CH_2CH_3)-$, $-CH(C_6H_5)CH_2CH_2O-$), 0.5–0.78 (m, $CH_3CH(CH_2CH_3)-$).

Polystyrene-b-poly(ethylene oxide)-b-polystyrene (SOS-1, SOS-1.6, SOS-2.3). SOS-1, SOS-1.6 and SOS-2.3 were prepared as described previously¹⁵ in which the alkoxide forms of SO-X diblock copolymers were coupled using dibromoxylene as a coupling agent. Crude reaction products included both SOS-Y triblock and residual SO-X diblock copolymer. Yields: 98+ % (containing SOS-Y and undesired SO-X). δH (400MHz, CDCl₃): 6.20–7.26 (br, $-C_6H_5$, $-OCH_2(C_6H_4)CH_2O-$), 3.1–4.0 (br, $-CH_2CH_2O-$, $-CH(C_6H_5)CH_2CH_2O-$), 1.0–2.30 (br, $-CH_2CH(C_6H_5)-$, $CH_3CH(CH_2CH_3)-$, $-CH(C_6H_5)CH_2CH_2O-$), 0.5–0.78 (m, $CH_3CH(CH_2CH_3)-$).

Fractionation. SOS-Y was isolated through fractionation of the crude product using chloroform/n-hexane as a solvent/non-solvent pair. The crude product was dissolved in chloroform in a beaker (1 wt% solution) and heated to 40 °C. n-hexane was added slowly to the slowly stirring polymer solution held at 40 °C until first detection of cloudiness. At that point stirring was stopped and the beaker was covered to prevent loss of solvent.

After several hours, the solution formed two separate layers. The upper layer was slowly decanted into another container leaving the sticky bottom layer behind. Both layers were redissolved, concentrated, and recovered through precipitation in pentane. Samples from both layers were characterized using SEC. Fractionation solutions were maintained above 40 °C to avoid solvent induced crystallization of PEO.¹¹ Several fractionations were typically repeated until the bottom layer contained 98% SOS-Y.

SO/SOS blend formation. Each sample was prepared by solution blending (0.2 g polymer per mL CHCl₃). The polymer mixtures were then freeze-dried using an ethanol/liquid nitrogen slush bath, and dried under vacuum at room temperature for at least 24 hours.

Polymer disk formation. Polymer disks of 8 mm in diameter and about 0.9 mm thick were melt pressed (Carver Press) using a stainless steel mold sandwiched between two pieces of Teflon[®] coated Kapton[®] sheets. The disks were held under a constant pressure of 500 psi at 150 °C for approximately 5 minutes before being removed. After cooling slowly to room temperature, the vitrified polymer disks were removed from the mold. The diameters and thicknesses of the disks were recorded for subsequent swelling experiments.

Swelling to equilibrium. Polymer disks were immersed in 125 mL of DI water (sealed jars) for at least 24 hours to ensure swelling equilibrium was reached. The jars were then placed in a large thermostated water bath held at the appropriate temperature (10 °C, 20 °C, 30 °C, 40 °C and 50 °C) for at least eight hours before any measurements were conducted on the hydrogels.

Characterization

Molecular characterization Size exclusion chromatography (SEC) was performed on a Viscotek GPC-Max chromatography system fitted with three 7.5 × 340 mm PolyporeTM (Polymer Laboratories) columns in series, an Alltech external column oven, and a Viscotek differential refractive index (RI) detector. S-OH molecular weight and polydispersity, and the polydispersity of the SO and SOS samples were determined using a THF (40 °C) mobile phase (1 mL min⁻¹) with PS standards (Polymer Laboratories). ¹H-NMR spectra were collected at room temperature in CDCl₃ on a Varian Inova 400 MHz spectrometer (n=32, delay=30s).

Small angle X-ray scattering (SAXS). SAXS data were collected on a Rigaku S-Max 3000 High Brilliance 3 Pinhole SAXS system outfitted with a MicroMax-007HFM Rotating Anode (CuK α), Confocal Max-FluxTM Optic, Gabriel Multiwire Area Detector and a Linkham thermal stage. Polymer disks described above were mounted on the thermal stage and heated to 120 °C, then cooled down to 100 °C and kept in vacuum for 120 minutes before exposure.

Determination of swelling ratio (Q). Hydrogels were removed from solution and quickly placed on a Teflon[®] surface. Excess water was gently blotted from the surface prior to

massing. This process was repeated four times. Hydrogels were returned to their thermostated DI solutions for at least one hour between each weighing.

Hydrogel rheology. Rheological tests were performed on a TA Instruments ARES rheometer with a customized recirculating bath fixture. In this test setup, an infinite lower plate (63 mm stainless steel) served as the bottom of an integrated glass cup, and the temperature of the lower plate was controlled by recirculating fluid through the base. Hydrogel samples at the desired equilibrated temperature were taken directly from the jars, blotted and placed at the center of the lower plate held at the same temperature. The hydrogels were compressed to their 90% of their equilibrium thicknesses to ensure good contact (no slip) between the hydrogel surface and parallel plates. Dynamic frequency sweeps (oscillatory shear) were performed for each sample using a 0.2-5.0 % shear strain (verified linear viscoelastic region) over a frequency range of 0.1 to 100 rad s⁻¹.

Results and discussion

Block Copolymer Synthesis. The syntheses of all SO diblock and SOS triblock copolymers were carried out using basic anionic polymerization techniques according to a previously reported multi-step protocol.^{15,20} The initial synthesis of a hydroxyl terminated polystyrene homopolymer was carried out in bulk quantities such that all subsequent diblock copolymers could be synthesized using the same S-OH macroinitiator. Coupling of SO diblock copolymer was used to generate SOS triblock copolymer, ensuring the symmetry of the block distribution with respect to the PS chain ends. The S-OH macroinitiator for all three SO-Y diblock copolymers was synthesized with a molecular weight of 8390 Da (SEC, PS standards) targeted to ensure a glass transition temperature above the PEO crystallization temperature (T_m, PEO ~ 65 °C, T_g, PS ~ 80 °C, Supporting information).²¹

This design criterion was enforced such that PS spherical domains assembled in the melt-state would have a chance to vitrify prior to the onset of PEO crystallization during sample cooling. Given the strong dependence of PS glass transition temperature on molecular weights below 10 kDa, the realistic lower limit for PS in these studies is in the 8 kDa range. This lower limit, in turn, dictates the formation of very large SO block copolymer molecules. That is, the consequence of utilizing the BCP spherical morphology is that very asymmetric molecules with low PS volume fractions ($f_{PS} = 0.08 - 0.13$) are required.^{22,23} To reach this level of asymmetry, the PEO block has to be very large (Table 1), even at the lower 8 kDa limit for the PS blocks. Three SO diblock copolymers were synthesized: SO-1, SO-1.6, and SO-2.3. SO-1 was synthesized to be the majority component in all SO-1/SOS-Y blends used in this study (Figure 1), and as the coupling precursor to the SOS-1 triblock copolymer. SO-1.6 and SO-2.3 were synthesized simply as precursors to triblock copolymers SOS-1.6 and SOS-2.3. The molecular weights of the

Table 1. Block copolymer characterization data

Sample Names	M_n (g/mol) ^a	$M_{n,PS}$ (g/mol)	$M_{n,PEO}$ (g/mol) ^d	f_{PS} ^c	PDI ^b
SO-1	84390	8390 ^b	76000	0.11	1.03
SO-1.6	129690	8390 ^b	121300	0.07	1.04
SO-2.3	183190	8390 ^b	174800	0.05	1.15
SOS-1	168780	16780 ^c	152000	0.11	1.10 ^f
SOS-1.6	259280	16780 ^c	242500	0.07	1.08 ^f
SOS-2.3	366380	16780 ^c	349600	0.05	1.08 ^f

^a The sum of the calculated PS and PEO molecular weights. ^b Determined from GPC (THF, PS std.). ^c Accounts for both PS chain ends. ^d Calculated from ¹H-NMR in combination with M_n of PS. ^e Volume fraction of PS, based on ¹H-NMR and nominal densities at 140 °C ($\rho_{PS}=0.969$, $\rho_{PEO}=1.064$ g/cm³).²⁴ ^f PDI of the fractionated SOS triblock copolymers.

SO-X diblock copolymers spanned the range of 76000 to 175000 g mol⁻¹ in this study. SEC of all diblock copolymers showed the absence of polystyrene homopolymer, confirming quantitative initiation from the alkoxide of the S-OH homopolymer. The molecular weights and volume fractions were calculated from ¹H-NMR peak integrations in combination with the known S-OH molecular weight established using SEC. Molecular weight distributions for both SO-1 and SO-1.6 diblock copolymers were very narrow as expected from the living chain kinetics of anionic polymerization. (PDI_{SO-1} = 1.03 and PDI_{SO-1.6} = 1.04). The polydispersity of SO-2.3 was slightly elevated, (PDI=1.15), a result that is consistent with the anionic polymerization of higher molecular weight PEO in THF solvent. This observation has been correlated to the changing solubility and equilibrium dynamics involving propagating species of differing ion pair associations, as molecular weights increase.²⁵ We have found lowering the polymer concentration in the reaction solution can improve PDI values.

SOS-Y triblock copolymers were synthesized from coupling the corresponding SO-X diblock copolymers, first forming the potassium alkoxide of the SO diblock copolymer and then using dibromoxylene (DBX) as a coupling agent. Coupling efficiencies were variable in the range of 44 - 84 wt%, but generally consistent with those traditionally achievable in large molecular weight systems.²⁶ The crude coupling reaction product contained both SOS triblock copolymer and partially reacted or unreacted SO diblock copolymer. Fractionation was used to isolate each of the triblock copolymers, SOS-1, SOS-1.6 and SOS-2.3 from their crude reaction mixtures. Fractionation was performed using chloroform/n-hexane as the solvent/non-solvent pair. Non-solvent addition was carried out holding the polymer solution at or above 40 °C to avoid (non)solvent-induced PEO crystallization. Previously reported to occur around 35 °C in chloroform/n-hexane solutions, such crystallization triggers generalized precipitation which is non-selective for SOS triblock copolymer.²⁷ The fractionation procedure was repeated multiple times to reduce SO-X content to less than 2 wt%. Data from repeated fractionations of SOS-1 are shown in Figure 2. The

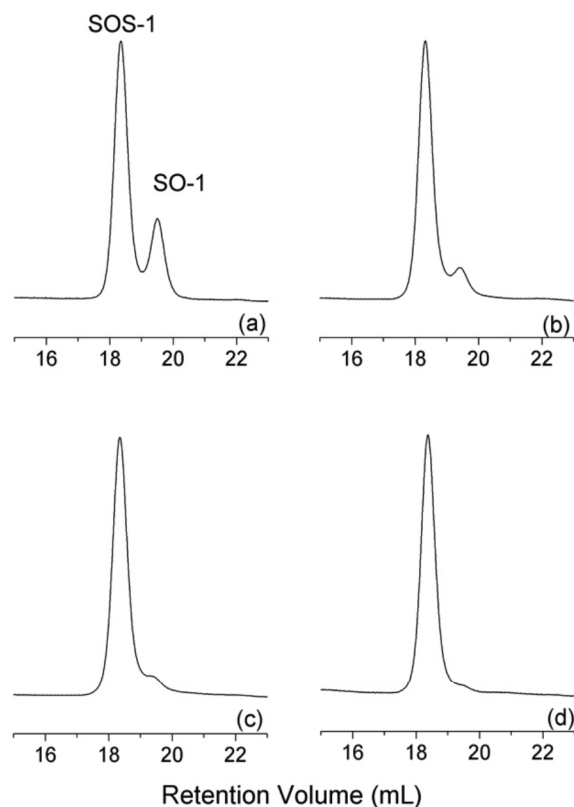


Figure 2. SEC data (in THF) from fractionation of the SOS-1 coupling reaction product. (a) Crude reaction product showing initial coupling efficiency. (b) First fractionation product (bottom layer). (c) Second fractionation product (bottom layer). (d) Third fractionation product (bottom layer).

original coupling reaction yielded approximately 84 wt% SOS-1, as shown in Figure 2(a). Figure 2(b), 2(c) and 2(d) represent the SEC traces of the fractionation product (bottom layer) collected after the first, second, and third fractionations. Fractionation of SO-1.6 and SO-2.3 produced similar results after a slightly larger number of fractionation cycles. Molecular weights and compositions of the isolated SOS-Y triblock copolymers remained consistent with the coupling of the SO-X diblock copolymers, as shown in Table 1. Interestingly, the fractionation decreased the PDI of triblock copolymer SOS-2.3 as compared with diblock copolymer SO-2.3, a likely result of both favorable coupling statistics and the subsequent fractionation processes.

Characterization of SO/SOS blends. The series of SOS-Y_x blends were prepared using simple solution blending in chloroform, with SOS-Y denoting the tether type and x representing the molar concentration (in mol%) of SOS-Y triblock copolymer in the sample. For each of the three SO-1/SOS-Y combinations outlined in Figure 1, blends were produced with 3.0, 5.0, 10.0, and 15.0 mol% SOS-Y. Importantly, in blends formed from the SO-1/SOS-1 pairing, the volume fraction of PS (f_{PS}) remains constant regardless of SOS-1 content, a consequence of the matched compositions of SO-1 and SOS-1. However, in blends formed from SO-1/SOS-1.6 or SO-1/SOS-2.3, the reduced PS content in the SOS component acts to lower the overall f_{PS} , relative to the matched SO-1/SOS-1 pair. This was

Table 2. Chemical and melt-state morphological characterization data of block copolymer blends

Sample	Diblock	Tether type	Tether added (mol%)	f_{PS}	Percus-Yevick hard sphere model				
					R_c^a/nm	ϕ_c^b	θ_{PS}^c	R_{hs}^d/nm	ϕ_{hs}^e
SOS-1_3	SO-1	SOS-1	3.0	0.11	9.2	0.097	227	16.6	0.57
SOS-1_5			5.0	0.11					
SOS-1_10			10.0	0.11					
SOS-1_15			15.0	0.11	9.4	0.099	242	16.7	0.56
SOS-1.6_3	SO-1	SOS-1.6	3.0	0.11	9.7	0.109	283	16.9	0.58
SOS-1.6_5			5.0	0.10					
SOS-1.6_10			10.0	0.10					
SOS-1.6_15			15.0	0.10	9.1	0.078	220	17.8	0.58
SOS-2.3_3	SO-1	SOS-2.3	3.0	0.10	9.7	0.104	283	16.8	0.54
SOS-2.3_5			5.0	0.10					
SOS-2.3_10			10.0	0.09					
SOS-2.3_15			15.0	0.08	9.5	0.082	250	17.4	0.50

^aMicelle core radius, ^bMicelle core overall volume fraction, $\phi_c = (R_c/R_{hs})^3 \phi_{hs}$, based on the PY parameters, ^cMean aggregation number (i.e., PS chains per sphere), based on the PY parameters, ^dapparent hard sphere radius, ^ehard sphere volume fraction.

of particular concern for the higher SOS-Y loadings, as a diminishing f_{PS} in the blends could begin to disfavor phase separation into the sphere-based morphology, a necessary constraint for tethered micelle network formation. Table 2 shows the f_{PS} values for each of the blends, which were ultimately maintained between 0.08 and 0.11.

While these values of f_{PS} were within the typical bounds for sphere formation in block copolymer melts,^{22,23} we chose to verify phase separation and spherical domain formation for all samples using SAXS. A subset of the SAXS results are plotted in Figure 3(a). Data for two blends, containing the lowest (3.0 mol%) and highest (15.0 mol%) SOS-Y amounts, are presented for each SO-1/SOS-Y combination. Notably, all blends share a common scattering profile which includes a prominent principal scattering peak at low values of the scattering wave vector q , followed by a less pronounced second broad peak at higher q

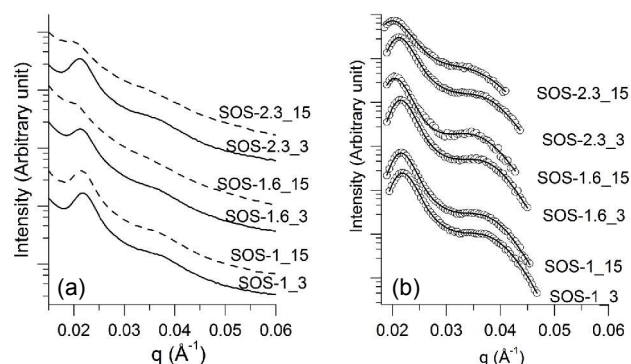


Figure 3. (a). SAXS data for melts (100°C) of SOS-1_3, SOS-1_15, SOS-1.6_3, SOS-1.6_15, SOS-2.3_3 and SOS-2.3_15 samples. (b). Background subtracted SAXS data (open circles) for SOS-1_3, SOS-1_15, SOS-1.6_3, SOS-1.6_15, SOS-2.3_3 and SOS-2.3_15 samples overlaid with nonlinear least square fits (solid line) to the Percus-Yevick hard sphere model for systems with liquid-like disorder.

values. This scattering signature is prototypical of sphere-forming block copolymer systems for which the packing structure of the micelle-like spherical domains can be described as "liquid-like". That is, due to the kinetic constraints associated with high molecular weight entanglements and limited macromolecular diffusion rates, these sphere-forming systems fail to develop a true bcc lattice that is typical in smaller molecular weight block copolymer systems.¹⁷ Simple comparisons of the relative positions of the principal scattering peaks in each of these samples reveals the qualitative impact of adding unmatched SOS triblock copolymer to the SO-1/SOS-Y blends.

Inspection of the matched SO-1/SOS-1 SAXS data shows that blends containing 3 mol% and 15 mol% SOS-1 give very nearly identical scattering, suggesting small amounts of matched triblock copolymer are largely inconsequential to the domain spacing produced during phase separation. This similarity is expected given the invariance of the blend composition to SOS-1 addition and the intrinsically matched lattice dimensions of the SO-1 and SOS-1 species in the self-assembled state. In contrast, increasing the amount of unmatched SOS-Y triblock copolymer in a blend with SO-1 does appear to have some influence on the characteristic dimensions of the system once the concentration is increased. At only 3 mol% SOS-1.6 or SOS-2.3, the additional PEO contributed by the SOS-Y is small and the characteristic dimensions are still dominated by SO-1. These systems still appear to structurally mimic the SO-1/SOS-1 blends. However, when the amount of SOS-1.6 or SOS-2.3 was increased to 15 mol%, the principal scattering peaks of both melt blends shifted to smaller q values (from $\sim 0.022 \text{ \AA}^{-1}$ to $\sim 0.021 \text{ \AA}^{-1}$), indicating increased PEO midblock molecular weights contributed by the SOS-Y triblock copolymer is pushing the average distance between PS cores to larger values. The exact source of this increase is impossible to characterize from the shift alone. That is, such a shift may be simply a result of the system expanding to accommodate the increase in PEO, but it may also be the result of PS cores of much higher aggregation number.

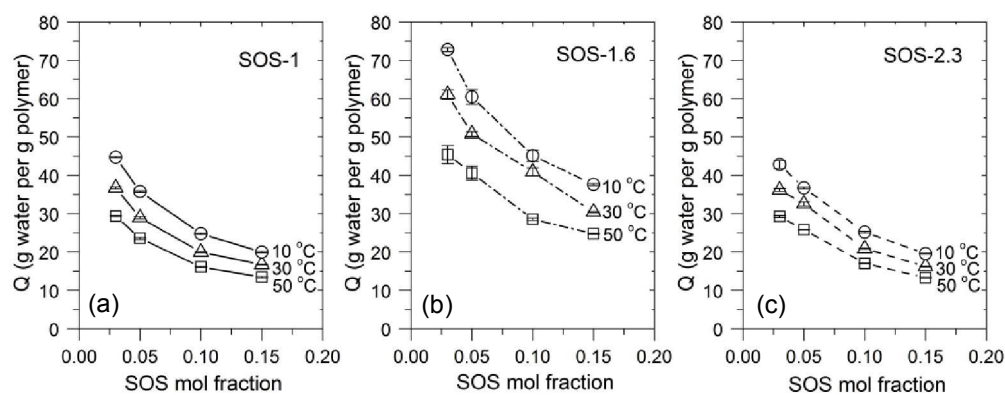


Figure 4. Equilibrium water content for combinations of SO-1 with (a) SOS-1, (b) SOS-1.6, and (c) SOS-2.3 at 10, 30 and 50 °C. All values determined gravimetrically. Error bars denote standard deviations from four measurements.

The scattering intensity for sphere forming systems can be expressed as a mathematical function which is proportional to the product of the form factor $P(q)$, which describes the intraparticle correlations, and the structure factor, $S(q)$, which describes the interparticle correlations. We were able to model the scattering data from these six data sets using $P(q)$ for polydisperse solid spheres coupled with $S(q)$ given by the Percus–Yevick (PY) model²⁸ for hard sphere liquids. Analysis of each of these data sets using fits to Percus–Yevick (PY) model adapted for polydisperse hard sphere liquids sheds a bit of light on the basic structural details of the liquid-like packing (LLP) of micelles in the melt state, and perhaps the origin of the principal peak shift upon addition of unmatched SOS-Y triblock copolymer to SO-1 blends.

The details of the PY model used to fit the SAXS data have been described in detail in our previous publication,¹⁵ and by others.^{29–32} Figure 3(b) gives the background subtracted SAXS data for the six blend samples, overlaid with nonlinear least squares fits to the adapted PY model. The values of the key physical parameters producing these fits are given in Table 2.

At the heart of PY model is the hard sphere radius, R_{hs} , and the hard sphere volume fraction, ϕ_{hs} . R_{hs} corresponds to the apparent radius over which the micelle acts as a hard sphere relative to other micelles, and therefore extends beyond the PS core to include a significant fraction of the dense PEO corona. The overall volume fraction of the sample occupied by these hard sphere constructs is then given by ϕ_{hs} . R_{hs} is related to the average spacing between micelle domains, and ϕ_{hs} provides information about how efficiently packed the micelles are. For example, hard spheres packed on a simple cubic lattice would produce a maximum packing fraction of $\phi_{hs} = 0.52$. A bcc lattice would produce $\phi_{hs} = 0.68$. Additionally, from the PY fit we are able to extract the radius of PS domains comprising the micelle core, R_c , and the volume fraction of PS in those micelle cores, ϕ_c . Deviations between the true PS volume fraction, f_{PS} , and ϕ_c are typically associated with the presence of free PS chain ends in the system.

Application of the PY model to the six blends shows the radii of the PS micelle cores, R_c , to vary over an particularly small range, bounded between 9.1 and 9.7 nm. These values lead to aggregation numbers in the mid 200's, as expected for spherical

aggregates produced through melt-state self-assembly. Importantly, the model fit predicts micelle core volume fractions, ϕ_c , that are very close to f_{PS} for each system, confirming the vast majority of the PS chain ends are likely phase segregated into the micelle cores. In addition, the apparent hard sphere radii, R_{hs} , for matched blends SOS-1_3 and SOS-1_15, and the unmatched blends of lowest SOS-Y content, SOS-1.6_3 and SOS-2.3_3, are remarkably similar, falling in the 16.6–16.9 nm range. This is consistent with the coherence of the principal peak positions in the SAXS data for these four blends. Likewise, in the unmatched blends of highest SOS-Y content, SOS-1.6_15 and SOS-2.3_15, the hard sphere radii increase to 17.8 and 17.4 nm, respectively. This increase, which is consistent with the shift in the principal scattering peak to lower q values, suggests the impact of the additional PEO in the added tethers is to swell the size of the coronal layer, albeit by just a small fraction. Finally, it is noteworthy that the hard sphere volume fractions, ϕ_{hs} , with the exception of the SOS-2.3_15 sample (0.50), all fall above the packing efficiency of a simple cubic system (0.52). While these values (0.54 – 0.58) remain substantially below that of the bcc lattice (0.68) adopted by smaller molecular weight systems, their packing efficiency suggests these systems still act as reasonably organized liquids.

Equilibrium swelling behavior. Polymer disks formed from each blends were swollen in water over a 24 hour period to ensure equilibrium was reached. Each hydrogel (12 samples in total) was weighed gravimetrically over 10 °C increments from 10 °C to 50 °C. The weights were measured four times for each hydrogel, to account for measuring errors associated with blotting to remove excess water. After each measurement, hydrogels were placed back in DI water and returned to a thermostatted water bath for at least one hour before the next measurement was performed. This was done to minimize error associated with losses due to evaporation or over-blotting during measurement. The equilibrium water content is described by the swelling ratio, Q , defined as the weight of water absorbed per unit weight of dry polymer.

Figure 4a-c shows the equilibrium water content for each hydrogel at 10 °C, 30 °C and 50 °C, organized by the SOS-Y triblock copolymer used in the blend. The results of equilibrium water content for hydrogels at 20 and 40 °C have been excluded

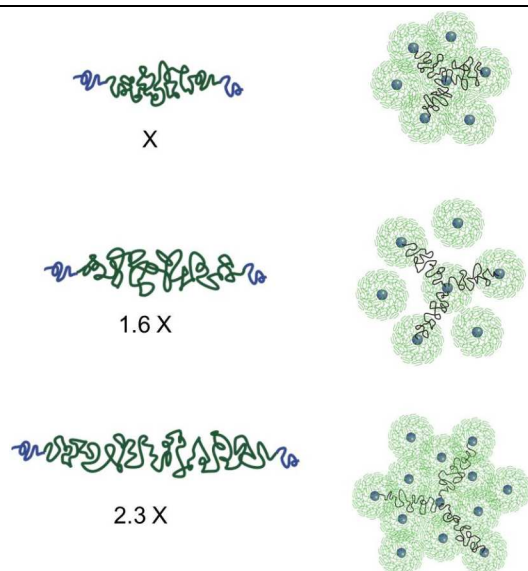


Figure 5. Proposed mechanism. When midblock size is 1X to 1.6X, the SOS triblock copolymers bridge only to the first shell of nearest neighbor micelles. Once the midblock molecular weight is increased to 2.3X, the SOS triblock copolymers are able to bridge into the second shell of nearest neighbor micelles.

for clarity. Globally speaking, as the temperature increased from 10 °C to 50 °C, about a 30 - 35% decrease in the water content was observed for all hydrogels. This is simply a result of the decreasing solubility of PEO in water with increasing temperature. Also, with increased concentration of SOS-Y from 3 to 15 mol%, about a 40 - 45 % decrease in the water content could be achieved. This is a direct result of the increased number of entanglements between the tethering midblocks of the bridging SOS triblock copolymer molecules, which scales with their concentration. Importantly, this behavior was across hydrogels from all SO-1/SOS-Y combinations investigated, and is consistent with the behavior observed in previous pre-structured hydrogels systems studied by our group.^{15, 17}

However, the impact of lengthening the tethering PEO midblock on the quantity of water absorbed by the hydrogel under equilibrium swelling conditions was rather remarkable. When the PEO midblock molecular weight was increased to 1.6 times (SOS-1.6_x hydrogels, Figure 4(b) the molecular weight of the matched system (SOS-1_x hydrogels, Figure 4(a)), swelling ratios of samples at identical SOS concentrations confirmed increases in water content ranging from 65 to 80 wt%. Interestingly, if the swollen dimensions of the hydrogel were determined solely by the tether adopting its preferred coil size in the presence of a theta solvent, we would expect a molecular weight increase of 1.6 times to coincide with the approximate doubling of the swelling ratio (100% increase). That these systems are able to achieve a considerable fraction of that given the constrained environment (entanglements with other tethers, fixed ends) inherent to these tethered micelle networks is quite impressive. Even at SOS loadings of 15 mol%, the additional swelling is consistently in this range. Rough estimates suggest the linear expansion of the hydrogel scales with the tether length to 0.35 - 0.42 power (cf. with 0.5 for a coil in a theta solvent), although the swelling results from the SOS-2.3 blends suggest the

application of that power law may have limitations (Vida infra).

As shown in Figure 4(c), an additional increase in the tether molecular weight to 2.3 times (SOS-2.3_x hydrogels) that of the matched system has a substantially different impact on the swelling of the hydrogel. The large increase in tether length does not continue to increase the equilibrium swelling ratio, but instead produces swelling capabilities comparable to that exhibited by the original matched SO-1/SOS-1 hydrogel blends. In fact, the swelling behavior at each concentration of SOS-2.3 was almost identical to the matched system at each temperature tested.

We believe these curious results can be interpreted using the organizational concepts outlined in Figure 5. For tethers of matched, or 1.6 times matched, molecular weights, the preferred melt-state conformation of the midblocks restricts bridging to nearest neighbor micelles only. As a result, the longer tether length can act to expand the inter-sphere distance during swelling. However, the increase to 2.3 times is sufficient to enable some fraction of the SOS-2.3 triblock copolymers to bridge into micelles occupying the shell of second nearest neighbors. Those chains in particular then act to restrict swelling to a state that more closely resembles the original capabilities of the matched SO-1/SOS-1 system. It is not clear at this point what tether length is sufficient to permit bridging to the second shell of nearest neighbors, whether the fraction of chains bridging to second shell matters, whether the transition to matched system swelling behavior is sharp or gradual in nature. Polydispersity in the mid-block is likely critical in the determination any of these swelling characteristics.

Impact on mechanical response. The mechanical response of each hydrogel under dynamic oscillatory shear at 30 °C is presented in Figure 6(a)-(c). Small strain values (0.2 - 5.0%) in the linear viscoelastic region were used to eliminate slip at the hydrogel-platen interface. Elastic moduli (G') for each hydrogel are plotted versus angular frequency in the range of 0.1 rad/s to 100 rad/s (see the ESI for an expanded version of Figure 6 complete with G'' data). As the plots show, the elastic moduli for all hydrogels at 30 °C were independent of frequency over the entire range tested. The impact of increasing the tether molecular weight from matched to 1.6 times matched is immediately evident, and quite dramatic. At equivalent concentrations of SOS triblock copolymer, increasing the tether length 1.6 times matched decreases the elastic modulus by almost a full order of magnitude. This substantial decrease has several implications concerning the origin of the elastic modulus in these tethered micelle networks. Clearly, the concentration of tethering molecules in and of itself is not the only factor determining the magnitude of the G' , given the equivalence in concentrations between the two systems. However, coupling this precipitous drop in modulus with the swelling data suggests that the proximity of the micelles in the network is critical in the determination of mechanical response. That is, when the tether lengths are matched in the system, the degree of coronal layer overlap is high, and the chain interactions (dynamic entanglements, e.g.) between those coronal layers dictates a majority of the elastic response (under small strain oscillation, at least). A comparison of the elastic moduli between hydrogels containing 15 mol% SOS-1 (4.8 kPa) and SOS-1.6 (0.51 kPa)

suggests that nearly 90% of the modulus (at least) originates from secondary network of tethers that would remain dormant until

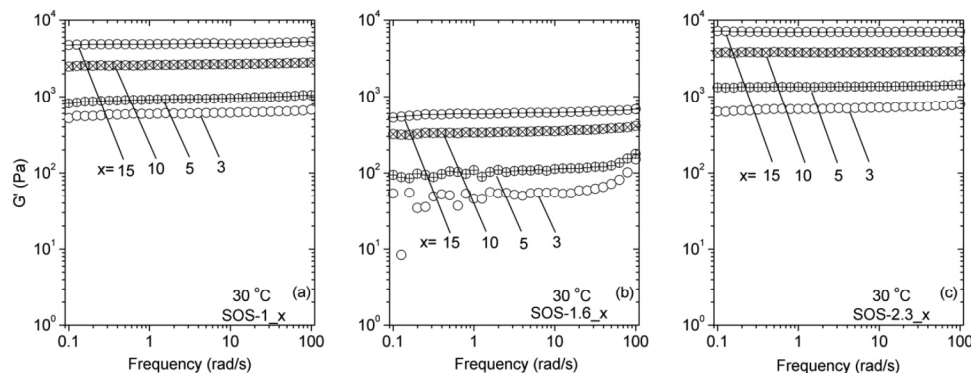


Figure 6. Dynamic frequency sweeps for hydrogels based on combinations of SO-1 with (a) SOS-1, (b) SOS-1.6, and (c) SOS-2.3 at 30 °C. "x" denotes the mol% SOS-Y triblock copolymer in the network. (see the ESI for an expanded version of Figure 6 complete with G'' data)

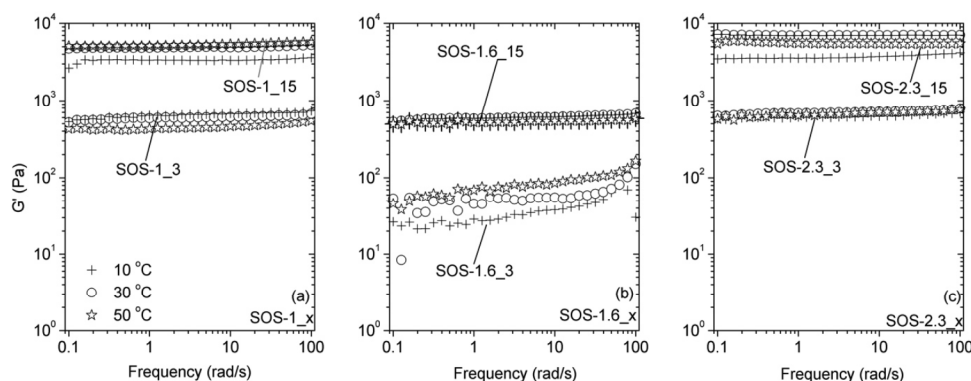


Figure 7. Dynamic frequency sweeps for hydrogels based on combinations of SO-1 with (a) SOS-1, (b) SOS-1.6, and (c) SOS-2.3 at 10, 30, and 50 °C. Data only for hydrogels containing 3 mol% and 15 mol% SOS-Y triblock copolymer in the network are shown. (see the ESI for an expanded version of Figure 7 complete with G'' data)

coronal layer interactions. This percentage assumes there is no residual coronal overlap still contributing to the elastic modulus in the SOS-1.6_15 sample. If that is untrue, this percentage may be even higher. Interestingly, the majority of chains comprising the coronal brush layer of PEO surrounding the PS core would be dangling ends in standard network nomenclature. Often, small concentrations of dangling ends are ignored because they have minimal influence on the mechanical properties of the network. However, in these tethered micelle systems, the concentration (and molecular weights) of these dangling ends is so high that their interactions actually dominate the mechanical behavior of the network.

Comparison with the SOS-2.3_x hydrogels appears to be consistent with the hypothesis put forward in Figure 5. As with swelling ratio, the use of the SOS-2.3 tethers produces dynamic elastic properties more reminiscent of the original matched SO-1/SOS-1 system, but in this case displaying about a 50% increase in elastic modulus when compared with matched systems of equal SOS content. We suspect this modest yet significant increase in modulus is attributable to the increased number of neighboring micelles to which each individual PS domain is mechanically correlated (connected) within the network. One could imagine that the inclusion of both SOS-1.6 and SOS-2.3 tethers in combination may present unique mechanical advantages for these hydrogel systems under tensile loading. The population of tethers formed by the SOS-1.6 might provide a

higher strains are reached. The potential of such systems to produce mechanically exceptional materials is the subject of future studies.

Finally, in Figure 7 we present the effect of temperature-induced swelling changes on the elastic moduli (G') of the hydrogel systems (see the ESI for an expanded version of Figure 7 complete with G'' data). Noticeably, there is no particular correlation with temperature that can be decoupled from simple sample-to-sample variation. Importantly, changing temperature (see Figure 4) has a significant effect on the water content in the hydrogel, with swelling ratios decreasing by up to 50%. However, the elastic modulus data in Figure 7 show that such large changes in water content from uniform expansion or contraction of the system do not influence the mechanical response to shear strain. It seems clear that while water intake does, for example, dilute the overall polymer concentration in the system, the simultaneous expansion of both the tethers and PEO coronal layers leaves the number of chain interactions between overlapping micelles essentially constant. We believe the significance of this data is that it underscores the minimal effects of water content, in and of itself, as a major contributor to the mechanical response of tethered micelle networks, and supports the contention that coronal layer overlap, for which temperature changes have very little effect, is the dominant factor in determining the dynamic mechanical response of these systems.

These results further emphasize the versatility of using melt-

state pre-structuring as a method through which one can access mechanically improved, tunable ABA-based tethered micelle hydrogel systems. The data presented show that a through a simple combination of tether concentration and tether length, the mechanical response of the resultant tethered micelle network can be tuned across a very significant range. The key is that both serve as simple knobs through which the coronal layer overlap in the system can be tuned. Furthermore, the tethered micelle networks fabricated in this manner appear to have a mechanical response that is largely invariant over the temperature ranges examined here. Obviously, the reliance on PS vitrification specific to this system has temperature limitations, but such can be overcome through alternate block selection and the use of chemical crosslinking.¹⁷ Notably, such control over mechanical properties is not easily possible using traditional solution-based assembly of tethered micelle networks.

In the greater picture, however, the role of coronal layer overlap in determining the mechanical potential of the network would seem to apply to all ABA-type tethered micelle systems regardless of assembly method. That is, even in solution assembled ABA systems, there is a distribution of bridging and looping chains that is entirely dependent on block copolymer concentration during gelation. Coronal layers in this case would be comprised of both looping and singly anchored ABA chains, and their proximity and interaction with adjacent coronal layers would still appear to be the prominent factor in determining mechanical potential in these systems. Notably, the reduced entanglements associated with looped chains may have a significant impact on modulus, but should not change the overall correlation with overlap. Accessing this potential would, of course, remain contingent on achieving core (junction) integrity that allows the network structure to be fully exploited.

Conclusions

In this report we used tethering molecules of different lengths to extend our understanding of mechanical property control in tethered micelle networks. The work is based on the use of a previously published solvent-free fabrication methodology exploiting the melt-state self-assembly of (lattice matched) sphere-forming SO diblock and SOS triblock copolymer blends. Importantly, solvent-free pre-structuring of tethered micelle networks via this approach is capable of producing highly elastic and mechanically improved tethered-micelle hydrogel systems not typically possible using solution assembly techniques. In this work, we focused on the influence of substituting non-lattice matched SOS triblock copolymer during the melt-assembly process on the subsequent hydrogel swelling and mechanical response. SAXS confirmed that addition of non-lattice matched SOS triblock copolymer could be accomplished to concentrations as high as 15 mol% without disrupting the ability of the system to adopt the sphere morphology in the melt-state. By introducing SOS triblock copolymer with PEO midblocks that were 1.6 times that of the lattice matched system, we were able to increase swelling ratios by 65 to 80% (up to 73 g H₂O/g polymer), and effectively eliminate coronal layer overlap between adjacent micelles. In doing so, we were able to establish coronal layer overlap as the primary contributing factor in determining the dynamic elastic moduli exhibited by the matched systems.

Extending the tether length to 2.3 times, in contrast, produced swelling and coronal layer overlap analogous to the lattice matched system. A moderate (50%) yet significant improvement in elastic modulus was also observed. We hypothesize that tethering molecules of that length are able to bridge into the second shell of nearest neighbor micelles, precluding any increased swelling capabilities and reproducing the overlap more representative of the matched system. The modest improvements in modulus are attributable to the increased number of neighboring micelles to which each individual PS domain is mechanically connected. Notably, we were able to show that either tether concentration or tether length can be used to provide control over coronal layer overlap, and provide avenues through which the system mechanical properties can be tuned. In contrast, temperature induced changes in swelling ratio had limited impact on mechanical response, due to limited effects on the degree of coronal overlap. While such control is a unique feature of the melt-state fabrication approach to tethered micelle networks, these conclusions should apply to any ABA-type tethered micelle network regardless of assembly protocol.

Acknowledgements

This material is based upon work supported by the National Science Foundation under Grant Nos. CBET-1160026 and DMR-0645781.

Notes and references

^a Department of Chemical & Biological Engineering, Colorado State University, 1370 Campus Delivery, Fort Collins, Colorado, 80523, USA. Fax: +1 9704917369; Tel: +1 9704914648; E-mail: travis.bailey@colostate.edu

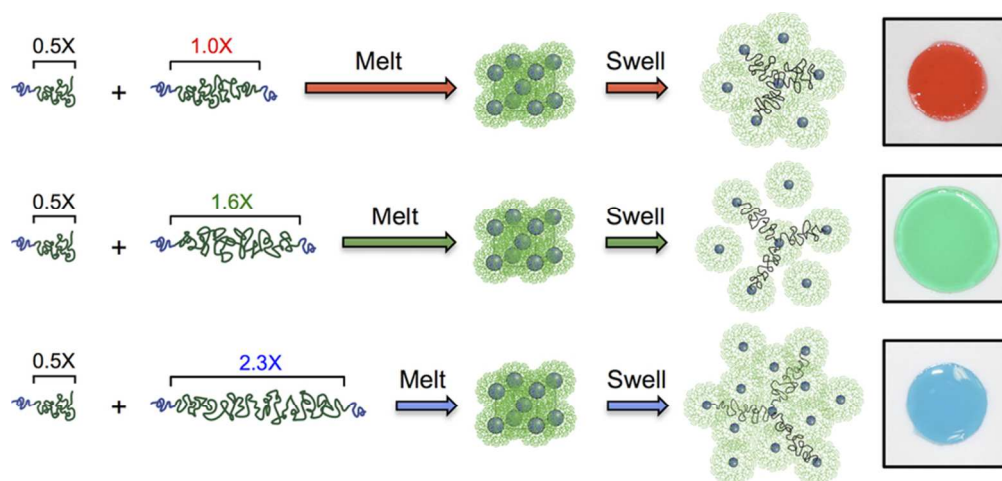
^b Department of Chemistry, Colorado State University, Fort Collins, Colorado, 80523. Fax: +1 9704911801; Tel: +1 9704916381

† Electronic Supplementary Information (ESI) available: [details of any supplementary information available should be included here]. See DOI: 10.1039/b000000x/

‡ Footnotes should appear here. These might include comments relevant to but not central to the matter under discussion, limited experimental and spectral data, and crystallographic data.

- Jeong, B.; Bae, Y. H.; Lee, D. S.; Kim, S. W. *Nature* **1997**, 388, (6645), 860-862.
- Yinghua Ma, Y. T., Norman C. Billingham, Steven P. Armes, Andrew L. Lewis. *Biomacromolecules* **2003**, 4, 864-868.
- Qiu, Y.; Park, K. *Advanced Drug Delivery Reviews* **2001**, 53, (3), 321-339.
- Jeong, B.; Bae, Y. H.; Kim, S. W. *Journal of Controlled Release* **2000**, 63, (1-2), 155-163.
- He, C.; Kim, S. W.; Lee, D. S. *Journal of Controlled Release* **2008**, 127, (3), 189-207.
- Kirkland, S. E.; Hensarling, R. M.; McConaughy, S. D.; Guo, Y.; Jarrett, W. L.; McCormick, C. L. *Biomacromolecules* **2008**, 9, (2), 481-486.
- Nguyen, K. T.; West, J. L. *Biomaterials* **2002**, 23, (22), 4307-4314.
- Drury, J. L.; Mooney, D. J. *Biomaterials* **2003**, 24, (24), 4337-4351.
- Kwon, I. K.; Matsuda, T. *Biomaterials* **2006**, 27, (7), 986-995.
- Aamer, K. A.; Sardinha, H.; Bhatia, S. R.; Tew, G. N. *Biomaterials* **2004**, 25, (6), 1087-1093.
- Fujiwara, T.; Mukose, T.; Yamaoka, T.; Yamane, H.; Sakurai, S.; Kimura, Y. *Macromolecular Bioscience* **2001**, 1, (5), 204-208.
- Park, K.; Kim, K.; Kwon, I. C.; Kim, S. K.; Lee, S.; Lee, D. Y.; Byun, Y. *Langmuir* **2004**, 20, (26), 11726-11731.
- Bromberg, L. *Macromolecules* **1998**, 31, (18), 6148-6156.

-
14. Sanabria-DeLong, N.; Crosby, A. J.; Tew, G. N. *Biomacromolecules* **2008**, 9, (10), 2784-2791.
 15. Guo, C.; Bailey, T. S. *Soft Matter* **2010**, 6, (19), 4807.
 16. Kissel, T.; Li, Y.; Unger, F. *Advanced Drug Delivery Reviews* **2002**, 54, (1), 99-134.
 - 5 17. Scalfani, V. F.; Bailey, T. S. *Macromolecules* **2011**, 44, (16), 6557-6567.
 18. Matsen, M. W.; Thompson, R. B. *The Journal of Chemical Physics* **1999**, 111, (15), 7139-7146.
 - 10 19. Paul C. Hiemenz, T. P. L., *Polymer Chemistry*. 2 ed.; CRC Press: 2007.
 20. R. P. Quirk, J. J. M. *Part A: Polym. Chem.* **1988**, 26, (8), 2031-2037.
 21. Blanchard, L.-P.; Hesse, J.; Malhotra, S. L. *Canadian Journal of Chemistry* **1974**, 52, (18), 3170-3175.
 - 15 22. Bates, F. S. *Science* **1991**, 251, 898-905.
 23. F. S. Bates, M. F. S., A. K. Khandpur, S. Foerster, J. H. Rosedale. *Faraday Discuss* **1994**, 98, 7-18.
 24. L. J. Fetters, D. J. L., D. Richter, T. A. Witten, A. Zirkel. *Macromolecules* **1994**, 27.
 - 20 25. Baskaran, D.; Muller, A. *Progress in Polymer Science* **2007**, 32, (2), 173-219.
 26. Nossarev, G. G.; Hogen-Esch, T. E. *Journal of Polymer Science Part A: Polymer Chemistry* **2001**, 39, (17), 3034-3041.
 - 25 27. Panagiota G. Fragouli, H. I., Nicko Hadjichristidis. *Polymer* **2002**, 7141-7144.



Changing tether length in melt-assembled hydrogel networks formed by sphere-forming AB and ABA block copolymer blends provides broad control over resultant swelling and mechanical properties.
39x19mm (600 x 600 DPI)